Black-hole quasinormal modes and scalar glueballs in a finite-temperature AdS/QCD model

JHEP11(2009)119

(http://iopscience.iop.org/1126-6708/2009/11/119)

Published by IOP Publishing for SISSA

Received: *September 10, 2009*
Accepted: *November 10, 2009*
Published: *November 27, 2009*

Black-hole quasinormal modes and scalar glueballs in a finite-temperature AdS/QCD model

Alex S. Miranda,[a] **C.A. Ballon Bayona,**[b] **Henrique Boschi-Filho**[a] **and Nelson R.F. Braga**[a]

[a] *Instituto de Física, Universidade Federal do Rio de Janeiro, Caixa Postal 68528, RJ 21941-972, Brazil*

[b] *Centro Brasileiro de Pesquisas Físicas, Rua Dr. Xavier Sigaud 150, Urca, 22290-180, Rio de Janeiro, RJ, Brazil*

E-mail: astmiranda@if.ufrj.br, ballon@cbpf.br, boschi@if.ufrj.br, braga@if.ufrj.br

Abstract: We use the holographic AdS/QCD soft-wall model to investigate the spectrum of scalar glueballs in a finite temperature plasma. In this model, glueballs are described by a massless scalar field in an AdS_5 black hole with a dilaton soft-wall background. Using AdS/CFT prescriptions, we compute the boundary retarded Green's function. The corresponding thermal spectral function shows quasiparticle peaks at low temperatures. We also compute the quasinormal modes of the scalar field in the soft-wall black hole geometry. The temperature and momentum dependences of these modes are analyzed. The positions and widths of the peaks of the spectral function are related to the frequencies of the quasinormal modes. Our numerical results are found employing the power series method and the computation of Breit-Wigner resonances.

Keywords: Gauge-gravity correspondence, AdS-CFT Correspondence, Phenomenological Models, Black Holes

ArXiv ePrint: 0909.1790v2

doi:10.1088/1126-6708/2009/11/119

JHEP11(2009)119

Contents

JHEP11(2009)119

1 Introduction

In the last years the AdS/CFT correspondence [1] has been recognized as an important tool to investigate diverse aspects of strongly coupled gauge theories. This correspondence relates a ten-dimensional string theory or eleven-dimensional M-theory to a conformal gauge theory on the corresponding spacetime boundary. The most celebrated version of this correspondence relates string theory in $AdS_5 \times S^5$ space to four-dimensional $SU(N_c)$ Yang-Mills gauge theory with large N_c and extended $\mathcal{N} = 4$ supersymmetry.

At low energy string theory is represented by an effective supergravity theory. Hence, the AdS/CFT correspondence implies a gauge/gravity duality. Using this duality, one can calculate quantities like quantum correlation functions for gauge-field boundary operators from the classical supergravity action for bulk fields [2, 3].

One can formulate a finite temperature version of the AdS/CFT correspondence including a black hole in the AdS spacetime. The Hawking temperature of the black hole,

related to the horizon position, is identified with the temperature of the dual gauge theory [4]. Following this approach, one can calculate various thermal Green's functions for the boundary gauge theory by taking derivatives of the on-shell bulk action for fields subjected to certain conditions. In the Euclidean version of the AdS/CFT correspondence, the prescription to compute Green's functions is the same found in [2, 3] with the classical bulk fields uniquely determined by their value at the boundary and the requirement of regularity at the horizon. In Minkowski space, a prescription for calculating retarded propagators at finite temperature was proposed in [5] (see also refs. [6–8]) imposing that the fields satisfy purely incoming-wave condition at the horizon. Physically, this means that the black holes only absorb without any emission. An important consequence of this prescription is that the poles of the retarded correlation function of an operator in the boundary conformal field theory correspond to the quasinormal (QN) frequencies of the holographic dual field in the AdS black-hole spacetime. In the context of the AdS/CFT correspondence, quasinormal modes have been object of study of many works (see ref. [9] for a recent review).

The AdS/CFT correspondence can be also an important tool to study many problems in strong interactions, like the calculation of hadronic spectra. The theory that describes strong interactions is QCD, a SU(3) Yang-Mills theory with a coupling constant that runs with the energy. At low energies the coupling is strong and one can not use perturbative methods. In this regime, one needs other approaches like lattice QCD or phenomenological effective models. Recently, the idea of modifying the AdS space introducing an infrared cut off led to phenomenological models to describe strong interactions. This modification implies a mass gap in the boundary gauge theory that breaks the conformal symmetry present in the AdS/CFT correspondence. This kind of approach is known as AdS/QCD.

The simplest AdS/QCD model, known as hard wall, introduces a mass gap via a cut off on the bulk geometry. In this way it is possible to use the gauge/gravity duality to estimate hadronic masses [10–15]. The hard wall is confining at low temperatures [16] and deconfining at high temperatures [17]. Another simple model of AdS/QCD, known as soft-wall, introduces a mass gap through a non-uniform background scalar field in the AdS spacetime. This soft-wall model presents linear Regge trajectories for vector mesons and glueballs [18–20]. Confinement/deconfinement thermal phase transition in these two models was studied in [21–24]. It was found in [22] that this corresponds to a gravitational Hawking-Page phase transition [25] between spaces with and without a black hole. This is a first order phase transition, where two different phases can coexist. The black-hole spacetime is thermally favored at high temperatures, while at temperatures below some critical model-dependent value, the thermally favored space is a pure AdS.

In this article we study the spectrum of scalar glueballs at finite temperature using the soft-wall AdS/QCD model. This model, at high temperatures, consists of an AdS space with a nonuniform background dilaton field and a black hole. At intermediate and low temperatures, we consider, respectively, the (supercooled) metastable and unstable phases of the plasma where the black hole is still present.[1]

[1] A similar situation was considered recently for the case of mesons in the D3-D7 model [26].

JHEP11(2009)119

Our motivation for studying the supercooled phase of the plasma is to gain some insight into the mechanism of glueball formation when the plasma cools down. We know that at the high temperatures reached when the plasma is formed, there are no stable hadronic states. On the other hand, at zero temperature, when the plasma disappears, there should be only colorless hadronic states with a well defined mass spectrum. These two separate regimes have been extensively studied using gauge/gravity duality. We want to investigate in this article how the transition between the high temperature deconfined phase and the zero temperature confined phase takes place. We think that this kind of analysis may be useful to understand hadronic formation in heavy ion collisions.

It is important to remark that the five dimensional background of the soft-wall phenomenological model does not arise as a solution of the 5D Einstein equations. In this model there is a time-independent background scalar field Φ that is a function of an infrared energy scale. In this article we will study the dynamics of an extra scalar field ϕ in this background at finite temperature. As the infrared energy scale goes to zero, the background Φ of the soft-wall model vanishes. In this limit, we recover the usual AdS/CFT picture and the scalar field ϕ can be thought as a perturbation of the trivial dilaton vacuum or of the scalar part of the metric. In the AdS/CFT correspondence this field is dual to the scalar glueball operator. Motivated by this fact, we assume in this work that the field ϕ is dual to scalar glueballs even in the presence of the infrared scale.

Therefore, we identify the quasinormal modes (QNM) of the massless scalar field in the bulk as the spectrum of scalar glueballs in the boundary. We study the zero- and finite-temperature retarded Green's functions of scalar glueball operators both with numerical and analytical techniques. The spectral function is identified with the imaginary part of the retarded Green's function. We perform also a numerical analysis to obtain the real and imaginary parts of the quasinormal frequencies as functions of the temperature and the spatial momentum. In such analysis a good convergence is achieved using the power series method [27] at high temperatures and the Breit-Wigner ressonance method [28] at low temperatures.

2 Glueballs in the soft-wall model at zero and finite temperature

In this section we obtain the equation of motion of a scalar field in the soft-wall model at zero and finite temperature and transform this equation into a Schrödinger-like form. We also describe the wave functions that are relevant for the computation of the glueball retarded Green's function and analyze the corresponding effective potential.

2.1 The soft-wall model at zero temperature

According to the AdS/CFT correspondence, the particle states on the boundary field theory are dual to normalizable fields in the bulk spacetime. As a consequence of the conformal symmetry, the mass spectrum of these states is continous. In the AdS/QCD models the conformal invariance is broken by the presence of an infrared cut-off turning the particle mass spectrum discrete. The soft-wall model of ref. [18] was originally formulated at zero temperature in order to reproduce the approximate linear Regge trajectories for vector

JHEP11(2009)119

mesons. It consists of a five-dimensional AdS spacetime and a background dilaton-like field $\Phi(z)$. The AdS_5 metric in Poincaré coordinates is given by

$$ds^2 = e^{2A(z)}\left[-dt^2 + \sum_{i=1}^{3}(dx^i)^2 + dz^2\right], \tag{2.1}$$

where $A(z) = -\ln(z/L)$ and L denotes the AdS curvature radius. The interaction of the background field $\Phi(z)$ with the bulk fields is defined through the replacement of the action integrals:

$$\int d^5x\sqrt{-g}\,\mathcal{L} \qquad \Longrightarrow \qquad \int d^5x\sqrt{-g}e^{-\Phi}\mathcal{L}\,. \tag{2.2}$$

The factor $\exp[-\Phi(z)]$ with $\Phi(z) = cz^2$ introduces an effective infrared cut-off in the AdS space, with $\sqrt{c}$ playing the role of a mass scale. This modifies the normalizability condition for bosonic fields in the bulk. The solutions with plane wave dependence $\exp(ik\cdot x)$ become normalizable only for particular discrete values of $k^2 = -m_n^2$, with nonvanishing m_n and $n = 0, 1, 2, \ldots$. This implies a mass gap in the dual gauge theory. For instance, the spectrum of vector mesons is [18]

$$m_{V_n}^2 = 4c(n+1)\,, \tag{2.3}$$

where n is the radial quantum number.

Scalar glueball states at zero temperature in the soft-wall model were studied in [19] by considering a massless scalar field living in the AdS spacetime (2.1) with the same dilaton background field $\Phi(z) = cz^2$. The corresponding glueball spectrum is

$$m_{G_n}^2 = 4c(n+2)\,. \tag{2.4}$$

The parameter $\sqrt{c}$, in this case, sets the scale of the glueball masses. Other recent results on glueballs in holographic models can be found in [29]. For a recent review on glueballs see [30].

2.2 The finite temperature case

The soft-wall model at finite temperature is composed by the dilaton field $\Phi = cz^2$ and an AdS black-hole spacetime with translationally invariant horizon:

$$ds^2 = e^{2A(z)}\left[-f(z)dt^2 + \sum_{i=1}^{3}(dx^i)^2 + f(z)^{-1}dz^2\right], \tag{2.5}$$

where $f(z) = 1 - (z/z_h)^4$. The coordinate z is defined in the range $0 \leq z \leq z_h$ and $z = 0$ corresponds to the boundary of the space. The parameter z_h indicates the position of the event horizon, which is related to the black-hole Hawking temperature T by $z_h = 1/\pi T$. According to the holographic dictionary, T also represents the temperature of the boundary field theory.

JHEP11(2009)119

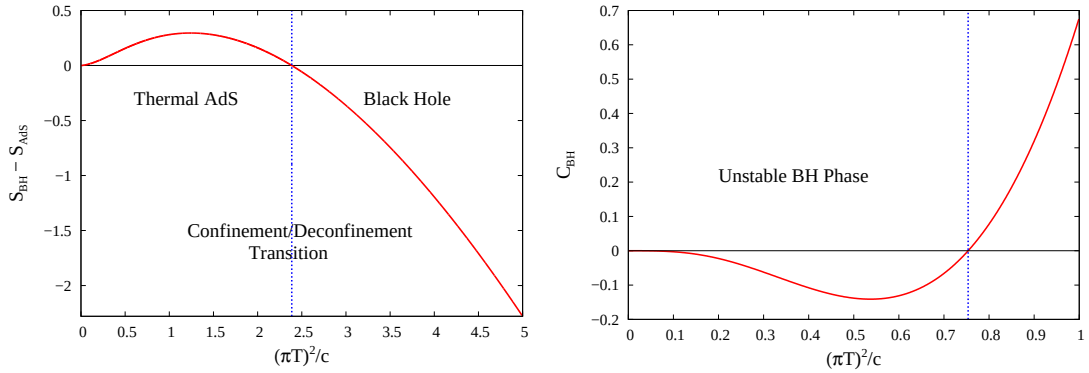

Figure 1. *Left*: Difference of regularized gravity action densities in the soft-wall model as a function of $(\pi T)^2/c$. *Right*: Specific heat density for the AdS black hole with the soft-wall dilaton as a function of $(\pi T)^2/c$. The quantities $S_{BH} - S_{AdS}$ and $\mathcal{C}_{BH}$ are in units of $N_c^2 c^{3/2}/4\pi$.

Thermodynamics

Considering the Euclidean version of the metrics given by (2.1) and (2.5) with compactified times, Herzog [22] has shown that, in the presence of the dilaton field $\Phi = cz^2$, there is a thermal competition between these spaces, which is characterized by the ratio $\widetilde{T} = \pi T/\sqrt{c}$. The regularized gravity action densities for the thermal AdS and AdS black hole spaces are given by [24]

$$S_{AdS} = \frac{N_c^2}{4\pi^2}\left[c^2\left(\frac{3}{2}-\gamma\right)\beta\right], \tag{2.6}$$

$$S_{BH} = S_{AdS} + \frac{N_c^2}{4\pi}\left[c^2 z_h Ei(-cz_h^2) + e^{-cz_h^2}\left(\frac{c}{z_h} - \frac{1}{z_h^3}\right) + \frac{1}{2z_h^3}\right], \tag{2.7}$$

where $Ei(u) = -\int_{-u}^{\infty} dt\, t^{-1} e^{-t}$ and $z_h = \beta/\pi$. At low temperatures the thermal AdS space is thermodynamically preferred compared to the AdS black-hole space, since it has a smaller gravity action. Then a first-order Hawking-Page type phase transition between these two spaces occurs at $\widetilde{T}_c^2 \approx 2.38644$. This transition is interpreted in the boundary field theory as a confinement/deconfinement phase transition as can be seen by calculating the corresponding entropy change. At $T > T_c$ the AdS black-hole space has a smaller gravity action so it is the dominant configuration. This space is dual to the plasma phase of a strongly coupled Yang-Mills theory with large number of colors. In the left panel of figure 1, we show the difference of the regularized gravity actions densities, $S_{BH} - S_{AdS}$, that determines the confinement/deconfinement phase transition.

In this article, we consider the black-hole spacetime (2.5) for all temperatures. For temperatures lower than T_c the black hole is not stable and can be interpreted as a super-cooled Yang-Mills plasma. If the sign of the specific heat is positive (negative) it will be in a metastable (unstable) phase. From the regularized action density for the soft-wall AdS black hole (2.7), we obtain the specific heat density

$$\mathcal{C}_{BH} \equiv -\beta^2 \frac{\partial^2}{\partial\beta^2} S_{BH} = \frac{\pi^2}{2} N_c^2 T^3 \left\{ e^{-\frac{c}{(\pi T)^2}} \left[\frac{4c}{(\pi T)^2} + 6\right] - 3 \right\}. \tag{2.8}$$

JHEP11(2009)119

In the limit $c \to 0$ we recover the usual (positive) result for the black hole without dilaton. In our case, the presence of the dilaton implies that the specific heat is negative for $\widetilde{T}^2 \lesssim 0.75$, as shown in the right panel of figure 1.

Equation of motion

The dual of the scalar glueball operator $\mathrm{Tr}(F^2)$ is a massless scalar field ϕ in the bulk. In the finite temperature soft-wall model this field is described by the action

$$S = -\frac{\pi^3 L^5}{4\kappa_{10}^2} \int d^5x \sqrt{-g} e^{-\Phi}\, g^{MN} \partial_M \phi \partial_N \phi \,, \tag{2.9}$$

where $\Phi(z) = cz^2$ is again the soft-wall dilaton field and g_{MN} is the black-hole metric given by (2.5). The constants L and κ_{10} are the anti-de Sitter radius and the ten-dimensional gravitational constant. The indices M, N run over $0, 1, \ldots, 4$ where x^μ $(\mu = 0, \ldots, 3)$ are the $4d$ boundary coordinates and $x^4 = z$ is the extra radial coordinate.

As usual in the soft-wall model, we do not consider here the backreaction of the dilaton Φ on the metric. From the action (2.9), we find the scalar field ϕ satisfies the equation

$$\frac{e^\Phi}{\sqrt{-g}} \partial_z \left(\sqrt{-g} e^{-\Phi} g^{zz} \partial_z \phi \right) + g^{\mu\nu} \partial_\mu \partial_\nu \phi \;=\; 0 \,. \tag{2.10}$$

Introducing the Fourier transform with respect to the coordinates x^μ,

$$\phi(z, x) = \int \frac{d^4k}{(2\pi)^4} e^{ik\cdot x} \bar{\phi}(z, k) \,, \tag{2.11}$$

equation (2.10) takes the form

$$e^B f(z) \partial_z \left(e^{-B} f(z) \partial_z \bar{\phi} \right) + \left(\omega^2 - f(z) q^2 \right) \bar{\phi} = 0 \,, \tag{2.12}$$

where $k_\mu = (-\omega, q_i)$, $q^2 = \sum_{i=1}^3 q_i^2$ and $B = \Phi - 3A = cz^2 + 3\ln(z/L)$.

2.3 The Schrödinger equation and the wave functions

In the study of classical-field perturbations around black holes, it is usually convenient to introduce the Regge-Wheeler tortoise coordinate r_*. This coordinate is defined by the relation $\partial_{r_*} = -f(z)\partial_z$ with z in the interval $0 \le z \le z_h$. Since in our case $1/f(z)$ is integrable we find the expression

$$r_* = \frac{1}{2} z_h \left[-\arctan\left(\frac{z}{z_h}\right) + \frac{1}{2} \ln\left(\frac{z_h - z}{z_h + z}\right) \right] . \tag{2.13}$$

Note that the horizon $z = z_h$ corresponds to $r_* \to -\infty$ and the boundary $z = 0$ is chosen at $r_* = 0$. It is also convenient to use a Bogoliubov transformation of the form $\psi = e^{-B/2}\bar{\phi}$. Then, eq. (2.12) reduces to a one-dimensional Schrödinger equation:

$$\partial_{r_*}^2 \psi + \omega^2 \psi = V\psi, \tag{2.14}$$

JHEP11(2009)119

where the effective potential V is given by

$$V = f(z)q^2 + e^{B/2}\partial_{r_*}^2 e^{-B/2}. \tag{2.15}$$

This potential can be explicitly written in terms of the coordinate z as

$$V(z) = \frac{f(z)}{z^2}\left[q^2 z^2 + \frac{15}{4} + \frac{9}{4}\frac{z^4}{z_h^4} + 2cz^2\left(1 + \frac{z^4}{z_h^4}\right) + c^2 z^4 f(z)\right]. \tag{2.16}$$

By investigating the asymptotic behavior of the Schrödinger equation (2.14) near the boundary $z = 0$ we find two particular real solutions ψ_1 and ψ_2. These solutions have the following asymptotic form:

$$\psi_1 = z^{5/2}\left[1 + a_{11}z^2 + a_{12}z^4 + \cdots\right], \tag{2.17}$$

$$\psi_2 = z^{-3/2}\left[1 + a_{21}z^2 + a_{22}z^4 + \cdots\right] + b\,\psi_1 \ln(cz^2), \tag{2.18}$$

where the ellipses denote higher powers of z and the coefficients above are given by

$$\begin{aligned} a_{11} &= -\frac{\omega^2 - q^2 - 2c}{12}, & a_{12} &= \frac{(\omega^2 - q^2 - 2c)^2}{12 \times 32} + \frac{1}{2z_h^4} + \frac{c^2}{32}, \\ a_{21} &= \frac{\omega^2 - q^2 - 2c}{4}, & b &= -\frac{(\omega^2 - q^2)(\omega^2 - q^2 - 4c)}{32}. \end{aligned} \tag{2.19}$$

The wave function ψ_1 is *normalizable* due to its asymptotic behavior $z^{5/2}$, while the wave function ψ_2 is *non-normalizable* since it behaves asymptotically as $z^{-3/2}$. The coefficient a_{22} is arbitrary and, in particular, we can choose $a_{22} = 0$. The solutions ψ_1 and ψ_2 will be useful to construct the glueball retarded Green's function in section 3, and to compute the black-hole quasinormal modes in section 4.

Another special kind of solutions to the Schrödinger equation (2.14) are the *ingoing* and *outgoing* wave functions, ψ_- and ψ_+. These solutions are motivated by the fact that the potential $V(z)$ vanishes when $z \to z_h$ so that eq. (2.14) takes the form of a free particle equation with solutions proportional to $\exp(\pm i\omega r_*)$. Since in our convention for the Fourier transform the temporal dependence of $\bar{\phi}$ is $\exp(-i\omega t)$, the minus (plus) sign can be interpreted as an ingoing (outgoing) plane wave in the sense that the wave travel into (out of) the horizon (localized at $r_* \to -\infty$) as the time increases. The solutions $\psi_\pm$ can be expressed in terms of the normalizable and non-normalizable solutions:

$$\psi_\pm = \mathcal{A}_{(\pm)}\psi_2 + \mathcal{B}_{(\pm)}\psi_1\,, \tag{2.20}$$

where $\mathcal{A}_{(\pm)}$ and $\mathcal{B}_{(\pm)}$ are connection coefficients associated to eq. (2.14), and determined as functions of ω and q by imposing the boundary conditions on the field solution.

The Schrödinger equation (2.14) can be expanded near the event horizon leading to the following expansion for ψ_- and ψ_+:

$$\psi_\pm = e^{\pm i\omega r_*}\left[1 + a_{1(\pm)}\left(1 - \frac{z}{z_h}\right) + a_{2(\pm)}\left(1 - \frac{z}{z_h}\right)^2 + \cdots\right], \tag{2.21}$$

JHEP11(2009)119

where the ellipses denote higher powers of $(1-z/z_h)$ and the coefficients appearing in the foregoing expression are

$$\begin{aligned} a_{1(\pm)} =& \frac{6+(q^2+4c)z_h^2}{4\pm 2i\omega z_h}, \\ a_{2(\pm)} =& \frac{1}{16\pm 4i\omega z_h}\Big\{\left[22\pm 4i\omega z_h+(q^2+4c)z_h^2\right]a_{1(\pm)}-2z_h^2(q^2+8c)-9+4c^2z_h^4\Big\}. \end{aligned} \tag{2.22}$$

The ingoing and outgoing wave functions form a basis for any other wave function. In particular, the normalizable and non-normalizable solutions ψ_1 and ψ_2 can be expressed as

$$\psi_2 = \mathcal{C}_{(2)}\psi_- + \mathcal{D}_{(2)}\psi_+\,, \qquad \psi_1 = \mathcal{C}_{(1)}\psi_- + \mathcal{D}_{(1)}\psi_+\,. \tag{2.23}$$

From (2.20) and (2.23) we find a useful relation between the connection coefficients

$$\begin{pmatrix} \mathcal{A}_{(-)} & \mathcal{B}_{(-)} \\ \mathcal{A}_{(+)} & \mathcal{B}_{(+)} \end{pmatrix} = \begin{pmatrix} \mathcal{C}_{(2)} & \mathcal{D}_{(2)} \\ \mathcal{C}_{(1)} & \mathcal{D}_{(1)} \end{pmatrix}^{-1}. \tag{2.24}$$

At zero temperature, it is not possible to impose the ingoing (outgoing) condition at the "horizon" $z=\infty$ due to the presence of the background dilaton field. Instead, we may impose the regularity condition

$$\lim_{z\to\infty}\psi_0 = 0\,, \tag{2.25}$$

where ψ_0 is a solution of eq. (2.14) at $T=0$. This wave function can be decomposed as

$$\psi_0 = \mathcal{A}_{(0)}\psi_2 + \mathcal{B}_{(0)}\psi_1, \tag{2.26}$$

where $\mathcal{A}_{(0)}$ and $\mathcal{B}_{(0)}$ are the zero-temperature connection coefficients associated to (2.14).

2.4 An analysis of the effective potential

We analyze here the effective potential $V(z)$, given explicitely by (2.16), as a function of r_*. At zero temperature ($z_h\to\infty$), the tortoise coordinate r_* reduces to $-z$ and the potential takes the form

$$V_{T=0}(z) = \frac{1}{z^2}\left[\frac{15}{4}+(q^2+2c)z^2+c^2z^4\right], \tag{2.27}$$

which is the potential considered in ref. [19], and that leads to the glueball spectrum of eq. (2.4). In a similar way, the limit $c\to 0$ reduces the effective potential to

$$V_{c=0}(z) = \frac{f(z)}{z^2}\left[q^2z^2+\frac{15}{4}+\frac{9}{4}\frac{z^4}{z_h^4}\right], \tag{2.28}$$

which is the potential obtained in refs. [31–33] in the absence of the dilaton. The effective potential $V(z)$ suffers a very interesting transition in shape when going from high to low temperatures. Such a transition is discussed below.

JHEP11(2009)119

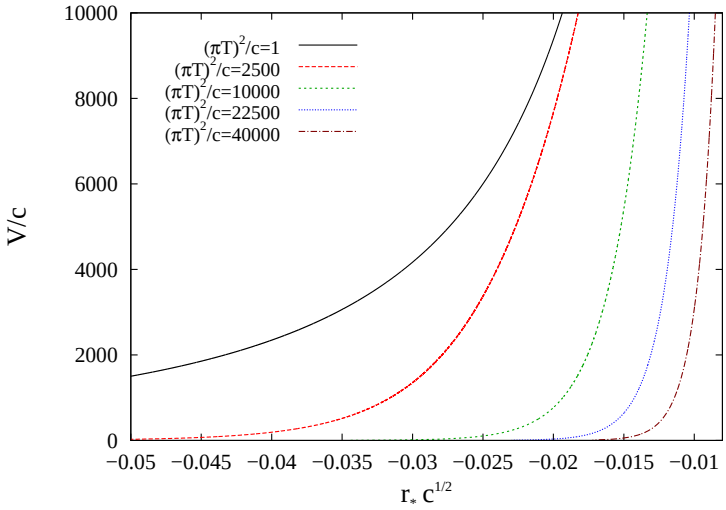

Figure 2. The behavior of the effective potential V for high- and intermediate-temperature values.

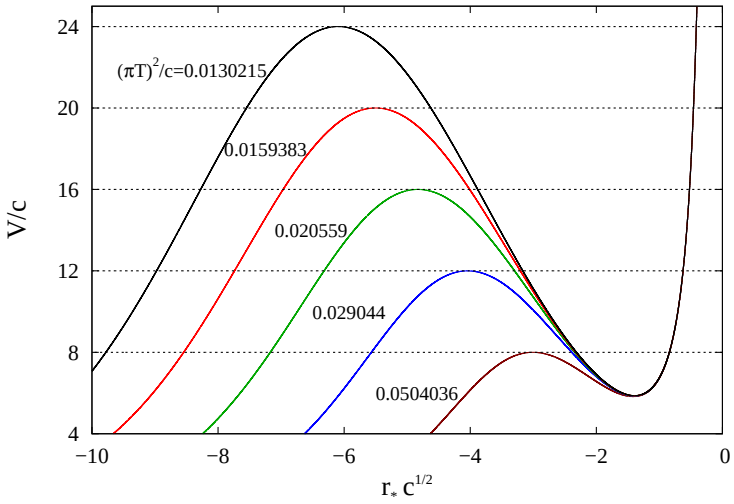

Figure 3. The behavior of the potential for low temperature values and $q = 0$. The horizontal dotted lines correspond to the masses of the glueball states at zero temperature.

High temperatures

In figure 2, we show the potential as a function of the tortoise coordinate in the high- and intermediate-temperature regimes for $q = 0$. We observe the absence of any potential well so that there are no bound states in these regimes. For any fixed value of the tortoise coordinate r_*, we note that the potencial increases with decreasing temperature. However, the shape of the potential does not change as one goes from high- to intermediate-temperature values. Therefore, on basis of the behavior of V, we do not expect a significative change in the spectrum of quasinormal modes as a function of temperature, for all $\widetilde{T}^2 \gtrsim 1$, in relation to the $\Phi = 0$ case.

JHEP11(2009)119

Low temperatures

At very low temperatures ($\widetilde{T}^2 \ll 1$), the effective potential begins to develop a well near the AdS boundary. This is illustrated in figure 3 where we plot the potential for some selected values of temperature and $q = 0$. As the temperature decreases the potential well gets deeper until it reaches the zero-temperature form. In the regime of low temperatures, the potential (2.16) with vanishing wavenumber can be approximated by

$$V = \frac{1}{z^2}\left[\frac{15}{4} - \frac{3}{2}\frac{z^4}{z_h^4} + 2cz^2 + c^2z^4 - 2c^2\frac{z^8}{z_h^4} + \mathcal{O}\left(\frac{z^8}{z_h^8}\right)\right], \tag{2.29}$$

where we have considered $(z/z_h)^4$ to be small, keeping only first-order terms in this parameter. The foregoing expression can be written in terms of the temperature as

$$V = \frac{15}{4z^2} + 2c + c^2z^2 - \left(\frac{3}{2} + 2c^2z^2\right) z^6\pi^4T^4\,, \tag{2.30}$$

where one can see explicitly the zero-temperature potential (2.27) plus low-temperature corrections, near the boundary. It is interesting to represent this potential in terms of the tortoise coordinate r_*. Near the boundary and for low temperatures, one can approximate the function $z(r_*)$ by

$$z = -r_*\left[1 - \frac{r_*^4}{5z_h^4}\right]. \tag{2.31}$$

Then, the potential (2.30) reads

$$V = 2c + c^2r_*^2 + \frac{15}{4r_*^2} - \frac{12}{5}c^2\,\pi^4\,r_*^6\,T^4\,. \tag{2.32}$$

The above potential is a combination of a constant term $2c$, an oscilator-like contribution proportional to r_*^2, an infinity barrier at $r_* = 0$, given by the term $15/4r_*^2$, and temperature dependent corrections. The negative sign of the thermal corrections, in the low-temperature regime, imply that the real part of the QN frequency ω will decrease with the temperature. Indeed, we will observe this behaviour in the study of the quasinormal modes in section 4.

An important consequence of the presence of the potential well at very low temperatures is the appearence of trapped modes. These modes are associated with scalar glueballs and will show up as peaks in the spectral function (the imaginary part of the Green's function) as will be discussed in the next section.

3 The retarded Green's function

In order to calculate the glueball retarded Green's function we follow the prescription of ref. [5]. First we use the equation of motion (2.10) to write down the on-shell version of the scalar field action (2.9):

$$S_{on\,shell} = \frac{\pi^3L^5}{4\kappa_{10}^2}\int d^4x\sqrt{-g}e^{-\Phi}\,g^{zz}\,\phi\,\partial_z\phi\,|_{z=0}\,, \tag{3.1}$$

JHEP11(2009)119

where we have disregarded the boundary term at the horizon $z = z_h$. The Fourier transformed on-shell scalar field $\bar{\phi}(z,k)$ is decomposed as

$$\bar{\phi}(z,k) = \phi_k(z)\phi_0(k), \tag{3.2}$$

where $\phi_k(z)$ is the "bulk to boundary propagator" subjected to the boundary condition

$$\lim_{z\to 0} \phi_k(z) = 1\,. \tag{3.3}$$

According to the Minkowkskian prescription of ref. [5], when computing the retarded Green's function one must consider a propagator $\phi_k(z)$ which satisfy an incoming-wave condition at horizon in the finite-temperature model,

$$\lim_{z\to z_h} e^{-\frac{cz^2}{2}} \left(\frac{z}{L}\right)^{-3/2} \phi_k(z) = \frac{1}{\phi_0(k)}\, e^{-i\omega r_*}\,, \tag{3.4}$$

or a regularity condition[2] at infinity ($z \to \infty$) in the zero-temperature case,

$$\lim_{z\to \infty} e^{-\frac{cz^2}{2}} \left(\frac{z}{L}\right)^{-3/2} \phi_k(z) = 0\,. \tag{3.5}$$

Using the decomposition (3.2), the action (3.1) takes the form

$$S_{on\ shell} = -\int \frac{d^4k}{(2\pi)^4}\, \phi_0(-k)\mathcal{F}(k,z)\, \phi_0(k)\,|_{z=0}\,. \tag{3.6}$$

The retarded Green's function is then given by

$$G^R(k) \equiv -2\,\mathcal{F}(k,z)\,|_{z=0} = \frac{\pi^3 L^5}{2\kappa_{10}^2} \lim_{z\to 0} \sqrt{-g}\, g^{zz} e^{-\Phi} \phi_k^*(z)\partial_z\phi_k(z)\,. \tag{3.7}$$

Since $\phi_k(z)$ is a solution of eq. (2.12) satisfying the normalization condition (3.3) and additionally the boundary condition (3.4) in the finite-temperature case and (3.5) in the zero-temperature case, it can expressed in terms of the wave functions defined in the last section as

$$\phi_k(z) = z^{3/2} e^{\frac{cz^2}{2}} \frac{\psi_a}{\mathcal{A}_{(a)}} = z^{3/2} e^{\frac{cz^2}{2}} \left[\psi_2(z) + \frac{\mathcal{B}_{(a)}}{\mathcal{A}_{(a)}}\psi_1(z)\right], \tag{3.8}$$

where the index a takes the value 0 for the zero temperature case and $-$ for finite temperature. Using the expansions (2.17) and (2.18) for ψ_1 and ψ_2, we find

$$G^R(k) = \frac{N_c^2}{8\pi^2}\left[(c+2a_{21})\epsilon^{-2} + 4b\ln(c\epsilon^2) + 2\left(b + a_{21}c + a_{21}^2\right) + 4\mathrm{Re}\frac{\mathcal{B}_{(a)}}{\mathcal{A}_{(a)}} - i\,\mathrm{Im}\frac{\mathcal{B}_{(a)}}{\mathcal{A}_{(a)}}\right], \tag{3.9}$$

where ϵ is an ultraviolet regulator. In the above equation we have used the relation

$$\frac{\pi^3 L^8}{2\kappa_{10}^2} = \frac{N_c^2}{8\pi^2}\,. \tag{3.10}$$

[2]The zero temperature condition (3.5) is equivalent to imposing the regularity condition $\lim_{z\to\infty}\phi_k(z) = 0$, for space-like momentum ($k^2 > 0$), and then performing a Wick rotation, similar to what was considered in ref. [5].

JHEP11(2009)119

The first two terms in eq. (3.9) are ultraviolet divergent and can be removed using a holographic renormalization procedure like that of ref. [34]. It is interesting to observe that the imaginary part of the retarded Green's function at zero (finite) temperature depends only on the quocient $\mathcal{B}_{(0)}/\mathcal{A}_{(0)}$ ($\mathcal{B}_{(-)}/\mathcal{A}_{(-)}$). This quantity defines the well-known spectral function which has been calculated in ref. [35] for vector mesons in the soft-wall model, and for other fields and holographic models, for example, in refs. [26, 36–39].

3.1 The zero-temperature case

In the zero temperature case, the bulk to boundary propagator has an analytical solution consisting on a combination of Kummer and Tricomi confluent hypergeometric functions. The Kummer function is ruled out by the regularity condition leading to

$$\phi_k(z) = \Gamma\left(\frac{k^2}{4c}+2\right)\, c^2\, z^4\, \mathcal{U}\left(\frac{k^2}{4c}+2\,,3\,,\, cz^2\right), \tag{3.11}$$

where $k^2 = -\omega^2+q^2$ and $\mathcal{U}(a,b,w)$ is the Tricomi function. From the asymptotic expansion of the Tricomi function we find near the boundary:

$$\begin{aligned} e^{-\frac{cz^2}{2}}\, z^{-\frac{3}{2}}\, \phi_k(z) \,=\, z^{-\frac{3}{2}} \Bigg\{ & 1 \,+\, a_{21} z^2 \,+\, b\, z^4\, \ln(cz^2) \\ & + \left[\frac{1}{8}+\frac{k^2}{8c}-\frac{k^2}{8c}\left(\frac{k^2}{4c}+1\right)\left(\Psi\left[\frac{k^2}{4c}+2\right]-\Psi(1)-\Psi(3)\right)\right] c^2\, z^4 \\ & + \mathcal{O}(z^6) \,+\, \mathcal{O}(\, z^6 \ln cz^2\,) \Bigg\}, \end{aligned} \tag{3.12}$$

where $\Psi(x)$ is the digamma function and a_{21} and b are given in eq. (2.19). From the above expansion we can extract

$$\frac{\mathcal{B}_{(0)}}{\mathcal{A}_{(0)}} \,=\, \left\{\frac{1}{8}+\frac{k^2}{8c}-\frac{k^2}{8c}\left(\frac{k^2}{4c}+1\right)\left[\Psi\left(\frac{k^2}{4c}+2\right)-\Psi(1)-\Psi(3)\right]\right\} c^2\,. \tag{3.13}$$

Since the digamma function $\Psi(x)$ has poles at $x = -n$, it is possible to extract an imaginary part of the retarded Green's function:

$$\begin{aligned} \mathrm{Im}\, G^R_{T=0}(k) \,&=\, -\frac{N_c^2}{8\pi^2}\,\mathrm{Im}\frac{\mathcal{B}_{(0)}}{\mathcal{A}_{(0)}} \,=\, \frac{N_c^2}{8\pi^2}\,\frac{k^2}{8c}\left(\frac{k^2}{4c}+1\right)\,\lim_{\epsilon\to 0}\,\mathrm{Im}\Psi\left(\frac{k^2}{4c}+2-i\epsilon\right) \\ &=\, \frac{N_c^2}{8\pi}\,\frac{k^2}{8c}\left(\frac{k^2}{4c}+1\right)^2 \sum_{n=0}^{\infty}\frac{1}{n+1}\delta\left(\frac{k^2}{4c}+2+n\right). \end{aligned} \tag{3.14}$$

Hence, the spectral function at zero temperature is a sum of delta functions localized at $k^2 = -4c(n+2)$. These poles are interpreted as the glueball masses at zero temperature. This result is consistent with the Feynman correlator obtained in ref. [40].

3.2 Spectral function at finite temperature

3.2.1 General procedure

In order to find the spectral function at finite temperature we must calculate the imaginary part of the retarded Green's function. We see from eq. (3.9) that $\mathrm{Im}\, G^R(k)$ depends on the

JHEP11(2009)119

ratio $\mathcal{B}_{(-)}/\mathcal{A}_{(-)}$, a quantity that can be calculated by a numerical procedure consisting in the steps described below.

Firstly, we solve numerically the Schrödinger equation (2.14) for a wave function that tends asymptotically to the normalizable solution $\psi_1(z)$ as $z \to 0$. In other words, we integrate numerically this equation from a point $z = z_i$ near the AdS boundary to a point $z = z_f$ near the horizon, using as "initial" conditions the truncated expansions

$$\psi_1(z_i) = z_i^{5/2}\left(1 + a_{11} z_i^2\right), \qquad \partial_z\psi_1(z_i) = \frac{1}{2}\, z_i^{3/2}\left(5 + 9\, a_{11} z_i^2\right). \tag{3.15}$$

The same numerical integration procedure is employed for a wave function that tends to the non-normalizable solution $\psi_2(z)$ as $z \to 0$. In this case, we use the following conditions near the boundary:

$$\begin{aligned} \psi_2(z_i) &= z_i^{-3/2}\left(1 + a_{21} z_i^2\right) + b\,\psi_1(z_i)\,\ln\left(c z_i^2\right), \\ \partial_z\psi_2(z_i) &= \frac{1}{2}\, z_i^{-5/2}\left[-3 + a_{21} z_i^2\right] + b\,\partial_z\psi_1(z_i)\,\ln\left(c z_i^2\right) + \frac{2b}{z_i}\,\psi_1(z_i). \end{aligned} \tag{3.16}$$

The expressions (3.15) and (3.16) are obtained from the near boundary asymptotic behavior for ψ_1 and ψ_2 discussed in the last section.

With the numerical results for ψ_1 and ψ_2 at $z = z_f$ we construct the vectors

$$\begin{pmatrix} \psi_j(z_f) \\ \partial_z\psi_j(z_f) \end{pmatrix} = \begin{pmatrix} \psi_-(z_f) & \psi_+(z_f) \\ \partial_z\psi_-(z_f) & \partial_z\psi_+(z_f) \end{pmatrix} \begin{pmatrix} \mathcal{C}_{(j)} \\ \mathcal{D}_{(j)} \end{pmatrix} \qquad (j = 1, 2)\,, \tag{3.17}$$

with $\psi_\pm(z_f)$ and $\partial_z\psi_\pm(z_f)$ given by the near-horizon expansions (2.21) truncated at second order in $(1 - z_f/z_h)$. Then we extract the coefficients $\mathcal{C}_{(j)}$ and $\mathcal{D}_{(j)}$ by inverting (3.17):

$$\begin{pmatrix} \mathcal{C}_{(j)} \\ \mathcal{D}_{(j)} \end{pmatrix} = \begin{pmatrix} \psi_-(z_f) & \psi_+(z_f) \\ \partial_z\psi_-(z_f) & \partial_z\psi_+(z_f) \end{pmatrix}^{-1} \begin{pmatrix} \psi_{(j)}(z_f) \\ \partial_z\psi_{(j)}(z_f) \end{pmatrix} \qquad (j = 1, 2). \tag{3.18}$$

Finally, from eqs. (2.24) and (3.18) we obtain

$$\frac{\mathcal{B}_{(-)}}{\mathcal{A}_{(-)}} = -\frac{\mathcal{D}_{(2)}}{\mathcal{D}_{(1)}} = \frac{\partial_z\psi_-(z_f)\psi_2(z_f) - \psi_-(z_f)\partial_z\psi_2(z_f)}{\partial_z\psi_-(z_f)\psi_1(z_f) - \psi_-(z_f)\partial_z\psi_1(z_f)}. \tag{3.19}$$

This way we can obtain numerically $\mathcal{B}_{(-)}/\mathcal{A}_{(-)}$ using the numerical results for ψ_1, ψ_2, $\partial_z\psi_1$ and $\partial_z\psi_2$ at a point $z = z_f$ near the horizon.

3.2.2 Numerical results

The imaginary part of the retarded Green's function gives us the spectral function

$$\mathcal{R}(\omega, q) \;\equiv\; -2\,\mathrm{Im}\, G^R(\omega, q) \;=\; \frac{N_c^2}{4\pi^2}\,\mathrm{Im}\frac{\mathcal{B}_{(-)}}{\mathcal{A}_{(-)}}\,. \tag{3.20}$$

We present here some numerical results for the spectral function obtained using the procedure discussed above. We show in figures 4 and 5 the dependence of the spectral function

JHEP11(2009)119

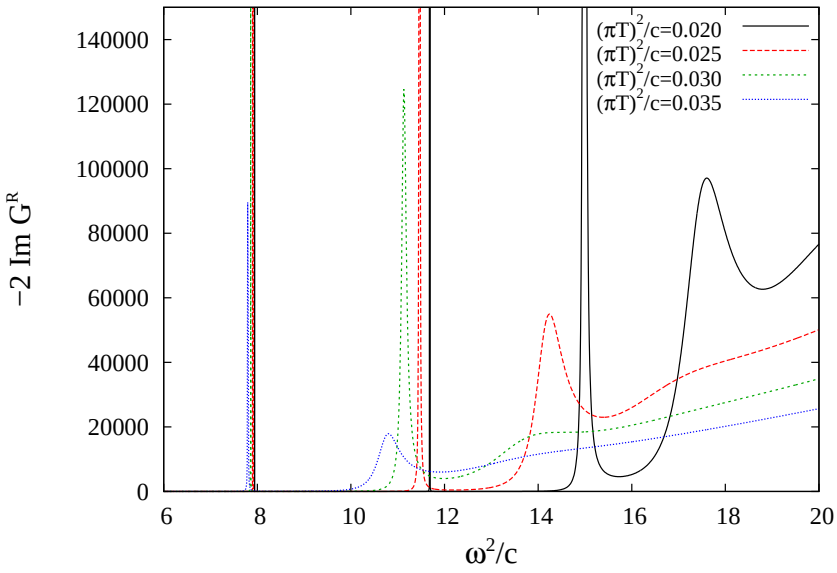

Figure 4. Spectral functions for $q = 0$ and selected values of temperature in units of $N_c^2/4\pi^2$. Note that the first peak of the spectral functions for the four cases almost coincide around $\widetilde{\omega}^2 = 8$.

with the frequency $\widetilde{\omega} = \omega/\sqrt{c}$ for selected values of temperature $\widetilde{T} = \pi T/\sqrt{c}$ and momentum $\widetilde{q} = q/\sqrt{c}$. We can see the presence of various peaks that correspond to the poles of the retarded Green's function. As commented above, these poles are associated with the frequencies of the black-hole quasinormal modes and are interpreted as glueball states in the dual gauge theory. Indeed, near one of the peaks the spectral function can be approximated by a Lorentzian function:

$$\mathcal{R}(\widetilde{\omega}, \widetilde{q}) \sim \frac{\widetilde{\omega}_I}{(\widetilde{\omega} - \widetilde{\omega}_R)^2 + \widetilde{\omega}_I^2}\,, \tag{3.21}$$

where $\widetilde{\omega}_R$ and $\widetilde{\omega}_I$ are respectively the real part and the negative of the imaginary part of the black-hole quasinormal frequencies. The half-width of the distribution (3.21), given by $\widetilde{\omega}_I$, is interpreted in the dual gauge theory as the inverse of the glueball lifetime (multiplied by the constant $\sqrt{c}$). The real part $\widetilde{\omega}_R$, for $q = 0$, gives a measure of the glueball mass at finite temperature.

We consider in figure 4 the zero-momentum case for various values of temperature. Note that as the temperature increases the number of peaks in the spectral function decreases while their width increase. Accordingly, the number of glueball quasiparticle states and their lifetimes decrease with the temperature. If we continue increasing the temperature we will reach a phase (for $\widetilde{T}^2 \gtrsim 0.1$) in which there are no more peaks. This suggests a kind of *glueball melting* in the sense that the glueball excitations disappear. A similar result was recently obtained in ref. [35] when studying finite-temperature effects on the spectrum of vector mesons in the soft-wall model. It is important to remark that for the range of temperatures in which we found glueball excitations (peaks in the spectral function), the theory is in an unstable phase.

JHEP11(2009)119

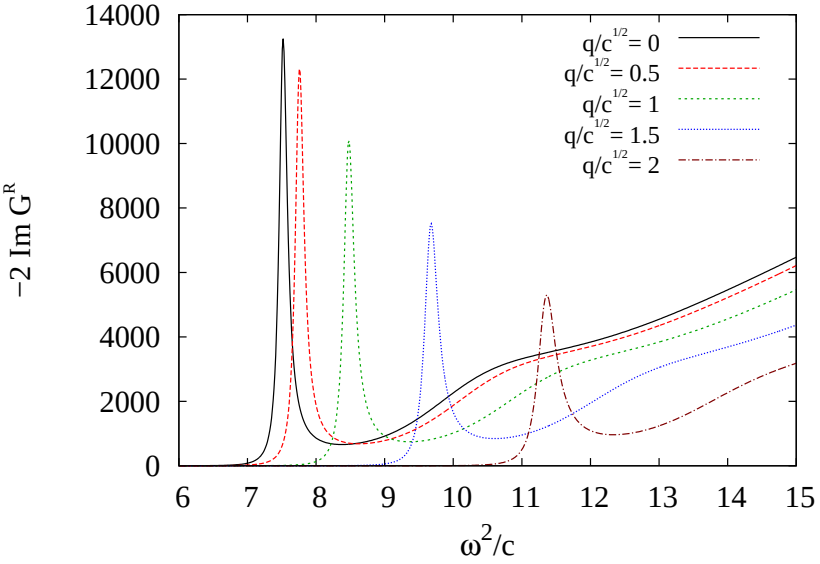

Figure 5. Spectral function for $\widetilde{T}^2 = 0.05$ and selected values of momentum $\widetilde{q}$ in units of $N_c^2/4\pi^2$.

It is interesting to analyze the spectral function of figure 4 on basis of the behavior of the effective potential of figure 3. For instance, for $\widetilde{T}^2 = 0.02$ there are three modes "trapped" in the potential well, which are represented by dotted lines. These quasi-stationary trapped modes correspond to the three sharp peaks that appear in the spectral function $\mathcal{R}(\widetilde{\omega}, 0)$. Analogously, for $\widetilde{T}^2 = 0.03$, the two sharp peaks at $\widetilde{\omega}^2 \approx 8$ and $\widetilde{\omega}^2 \approx 11$ are associated to the modes trapped in the potential well.

Note that the dotted lines shown in the effective potential graph of figure 3 correspond to the zero temperature modes. However, as shown in figure 4, the masses of the glueballs, given by the positions of the peaks, vary with the temperature. Nevertheless, this effect does not change the qualitative analysis made above.

Another important feature shown in figure 4 is that, for a fixed temperature, the width of the peaks increases with the frequency. This can be explained in terms of the tunneling effect of the scalar-field waves in the potential barriers of figure 3, which is enhanced when the frequency becomes comparable with the height of the potential well. Then, the glueball states at finite temperature become less stable as the energy increases.

In figure 5, we plot the spectral function for a fixed value of temperature $\widetilde{T}^2 = 0.05$ and various values of wavenumber $\widetilde{q}$. In this picture one can see that the position and the width of the peak increases with the momentum. This result indicates that the glueball energy increases with the momentum, as expected, while the glueball lifetime decreases.

In this section the frequency ω was taken as a real quantity for the computation of the spectral function $\mathcal{R}(\widetilde{\omega}, \widetilde{q})$. However, when studying the black-hole quasinormal modes (the poles of G^R) in the next section, we will look for frequencies of the form $\widetilde{\omega}_{QN} = \widetilde{\omega}_R - i\,\widetilde{\omega}_I$ with $\widetilde{\omega}_R$ and $\widetilde{\omega}_I$ being (positive) real quantities.

JHEP11(2009)119

4 Quasinormal modes and the scalar glueballs at finite T

Quasinormal modes (QNMs) are solutions for classical field perturbations on a black hole geometry (see refs. [9, 41, 42] for general reviews on the subject). These solutions are subjected to an absorption condition at the horizon and a regularity condition at the spacetime boundary in the AdS black hole case. The absorption condition leads to a purely ingoing wave at the horizon while the regularity at the boundary translates into a Dirichlet condition for ψ, for the case of a massless scalar field discussed here.

The analysis of the effective potential in section 2 gives additional support to the above quoted boundary conditions. The fact that the effective potential diverges at the spacetime boundary $z = 0$ makes it natural to impose a Dirichlet condition, while the vanishing of the potential at $z = z_h$ and the one-way membrane property of the horizon lead naturally to ingoing plane wave solutions.

The absorption condition can be implemented by means of the solution $\psi_-(z)$ of section 2, which behaves like an ingoing wave at the horizon, according to eq. (2.21). Imposing Dirichlet boundary condition on $\psi_-(z)$ at $z = 0$ implies that the connection coefficient $\mathcal{A}_{(-)}(\omega, q)$ vanishes. Since the retarded Green's function (3.9) diverges when $\mathcal{A}_{(-)}(\omega, q) = 0$, we conclude that the *black-hole quasinormal modes* correspond to the (complex) poles of the glueball retarded Green's function.

In the following, we will show the numerical results obtained for the complex roots $\omega_{QN} = \omega_R - i\,\omega_I$ of the equation $\mathcal{A}_{(-)}(\omega, q) = 0$. These complex roots are the frequencies of the scalar-field quasinormal modes of the black hole in the presence of the soft-wall dilaton background. Previous studies of quasinormal modes in the context of gauge/gravity duality can be found, for example, in refs. [27, 43–55].

4.1 Methods

In the last decades, different methods have been developed to numerically calculate the quasinormal modes of black holes. We employ here two of these techniques to find out the QNMs of a scalar field in the soft-wall model. The first one is the traditional Fröbenius power series method, following the approach of Horowitz and Hubeny [27]. In this case the problem of finding quasinormal frequencies is reduced to that of finding the roots of a polynomial equation. The second method is based on ideas from the study of the ressonant scattering problem in atomic and nuclear physics. It has been recently applied to the calculation of QNMs [28] and is presently known as the Breit-Wigner resonance method.

4.1.1 The power series method

The power series method of ref. [27] is of particular interest for the present work since it is suited for asymptotically AdS spacetimes. We start with the scalar field equation of motion written as a Schrödinger-like equation (2.14). As discussed above, QNMs are defined as solutions which are purely ingoing waves at horizon, $\psi \to \mathrm{e}^{-i\omega r_*}$, and satisfy a Dirichlet condition at $z = 0$. In the power series method, it is convenient to introduce a

JHEP11(2009)119

new function $\varphi = e^{+i\omega r_*}\psi$. Then, eq. (2.14) becomes

$$f(z)\,\frac{d^2\varphi}{dz^2} + \left(2i\omega - 4\frac{z^3}{z_h^4}\right)\frac{d\varphi}{dz} - \frac{V(z)}{f(z)}\,\varphi = 0\,. \tag{4.1}$$

The above equation has a regular singular point ($z = z_h$) in the region of interest, $0 \leq z \leq z_h$. So, according to the Fuchs's theorem, at least one of the solutions of eq. (4.1) can be written as a Fröbenius series [56]. In fact, from the solution (2.21) for ψ_- one can see that the corresponding function φ_- can be written as a power series of the form:

$$\varphi_-(z) = \sum_{m=0}^{\infty} a_{m(-)} \left(1 - \frac{z}{z_h}\right)^m . \tag{4.2}$$

Substituting eq. (4.2) into (4.1) we obtain a recurrence relation for the coefficients a_m's. Since eq. (4.1) is linear we can set $a_0 = 1$ and calculate this way any coefficient $a_{m(-)}$ as a function of the frequency $\widetilde{\omega} = \omega/\sqrt{c}$, the wavenumber $\widetilde{q} = q/\sqrt{c}$, and the temperature $\widetilde{T} = \pi T/\sqrt{c}$. The coefficients $a_{1(-)}$ and $a_{2(-)}$ are given explicitly in equation (2.22). Then, imposing the Dirichlet condition at AdS boundary, we obtain

$$\varphi_-(0) = \sum_{m=0}^{\infty} a_{m(-)} = 0. \tag{4.3}$$

Thus, the problem of finding quasinormal (QN) frequencies has been reduced to that of obtaining the roots of the equation (4.3). Since we cannot carry out numerically the full sum in expression (4.3), we truncate the series after a large number of terms and look for the zeros of the resulting partial sum. The precision of the results is then verified through the relative variation between the roots of two successive partial sums. For each pair of $\widetilde{q}$ and $\widetilde{T}$, we find a set of QN frequencies $\widetilde{\omega}$, labeled by the principal quantum number n and ordered in a set beginning by the roots with the lowest absolute values for the imaginary part.

4.1.2 The Breit-Wigner method

Although the power series method is suitable to find QN frequencies in the intermediate- and high-temperature regimes ($\widetilde{T} \gtrsim 1$), its convergence gets weak at very low temperatures ($\widetilde{T} \ll 1$). Fortunately, in this regime the behavior of the effective potential $V(r_*)$ enable us to use an alternative method based on the Breit-Wigner theory of resonances.

The theory of Breit-Wigner resonances was originally employed in gravitational problems to find the resonant frequencies associated with ultra-compact relativistic stars [57–59], and only recently this technique was used to find QN frequencies of black holes, particularly of very small Schwarzschild-AdS black holes [9, 28]. An important element for the efficiency of this method is the form of the effective potential: $V(r_*)$ should have the form of a very deep well, so that quasi-stationary "trapped" states can exist and the scalar field waves can only leak out to the horizon by tunneling through the potential barrier. This is exactly the situation found in section 2 when analyzing the effective potential for a massless scalar field in the soft-wall black hole geometry. Below we present the general idea of this method in the form used in asymptoticaly AdS spacetimes.

JHEP11(2009)119

The resonance method deals with normalizable solutions, which corresponds here to choosing the solution ψ_1 of eq. (2.17). As discussed in section 2, the function ψ_1 can be written as a combination of *ingoing* and *outgoing* waves $\psi_\pm$, as shown in eq. (2.23). This equation determines the asymptotic behavior of ψ_1 at the horizon:

$$\psi_1 = \mathcal{C}_1 e^{-i\omega r_*} + \mathcal{D}_1 e^{i\omega r_*} = \alpha \cos\omega r_* + \beta \sin\omega r_*, \tag{4.4}$$

where $\alpha = \mathcal{C}_1 + \mathcal{D}_1$ and $\beta = -i(\mathcal{C}_1 - \mathcal{D}_1)$. The QNMs are normalizable solutions with complex frequencies $\omega_{QN} = \omega_R - i\,\omega_I$ such that there are no outgoing waves. This corresponds to set $\mathcal{D}_1 = 0$. Analogously, the complex conjugate of a QNM corresponds to the vanishing of the ingoing coefficient ($\mathcal{C}_1 = 0$). Assuming that the QNMs are simple zeros of $\mathcal{D}_1$ we expect that near these modes $\mathcal{D}_1 \sim (\omega - \omega_R) + i\omega_I$ and $\mathcal{C}_1 \sim (\omega - \omega_R) - i\omega_I$. Then it turns convenient to introduce the real quantity

$$\alpha^2 + \beta^2 = 4\mathcal{C}_1\mathcal{D}_1 \approx \text{const.} \times \left[(\omega - \omega_R)^2 + \omega_I^2\right]. \tag{4.5}$$

The Breit-Wigner resonance method is based on the minimization of this quantity, considering ω as a real variable [57, 59]. Note that this is far simpler than solving the complex equation $\mathcal{D}_1 = 0$ when using the numerical integration procedure of section 3.

The quantity $\alpha^2 + \beta^2$ will present sharp dips at $\omega = \omega_R$ corresponding to the real parts of the QN frequencies. Once we have located a minimum of $\alpha^2 + \beta^2$ on the line of real ω at some $\omega = \omega_R$, the imaginary part of the QN frequency ω_I is obtained by means of a parabolic fit of the Breit-Wigner formula (4.5). To set the accuracy of our numerical results, we use the alternative (and equivalent) expressions for ω_I:

$$\omega_I = -\beta/\alpha' = \alpha/\beta', \tag{4.6}$$

where a prime indicates a derivative with respect to ω_R, evaluated at the minimum [28, 58]. The Breit-Wigner method has, in general, a good convergence as long as the condition $\omega_I \ll \omega_R$ is satisfied.

It is interesting to notice the relation between the dips of $\alpha^2 + \beta^2$ and the peaks of the spectral function $\mathcal{R}(\omega, q)$, discussed in section 3. Each minimum of (4.5) appears as a sharp maximum of the spectral function. This connection can be understood by considering the approximate expression

$$\mathcal{R} = -2\text{Im}G^R \sim (\mathcal{A}_{(-)})^{-1} \sim (\mathcal{D}_1)^{-1}. \tag{4.7}$$

Therefore, the simple pole hypothesis for the retarded Green's function that leads to (3.21) is directly related to the simple zero hypothesis for the coefficient $\mathcal{D}_1$.

4.2 Numerical results for the QN frequencies

4.2.1 Temperature dependence

Here we present our numerical results for the QN frequencies when varying the temperature while keeping the momentum $q = 0$. The power series method can be applied to a wide range of values from high temperatures to $\widetilde{T}^2 \approx 0.022$. At lower temperatures, the power

JHEP11(2009)119

	Power series		Breit-Wigner	
$\widetilde{T}^2$	$\widetilde{\omega}_R^2$	$\widetilde{\omega}_I^2$	$\widetilde{\omega}_R^2$	$\widetilde{\omega}_I^2$
0.0493827	7.52779	1.41127×10^{-4}	7.53270	1.43646×10^{-4}
0.04	7.72086	1.31516×10^{-6}	7.72092	1.31549×10^{-6}
0.0330579	7.82420	2.12446×10^{-9}	7.82420	2.12446×10^{-9}
0.0277778	7.88073	8.61149×10^{-13}	7.88073	8.61151×10^{-13}
0.0236686	7.91529	1.04760×10^{-16}	7.91529	1.04873×10^{-16}
0.0204082	—	—	7.93787	2.23960×10^{-20}

Table 1. A comparison between the values obtained for the fundamental ($n = 0$) QN frequency computed using the power series and the Breit-Wigner resonance methods.

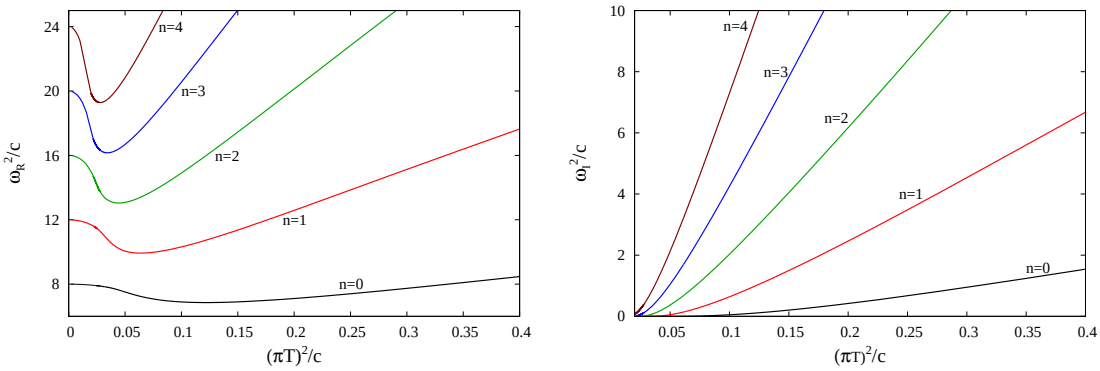

Figure 6. Numerical results for the square of the real and imaginary parts of the QN frequencies, ω_R^2/c and ω_I^2/c, for the first five quasinormal modes $n = 0, 1, \ldots, 4$, with $q = 0$.

series method has convergence problems but, as we discussed above, it is precisely in this regime that the wells of the potential are deep and the dips in $\alpha^2 + \beta^2$ are sharp enough to make the Breit-Wigner method efficient. We have used the Breit-Wigner method for $\widetilde{T}^2 \lesssim 0.05$. A comparison of the results obtained with the two methods is presented in table 1. The approaches are complementary, and show a very good agreement for the range $0.025 < \widetilde{T}^2 < 0.04$.

The values of $\widetilde{\omega}_I$ shown in table 1 for the Breit-Wigner method were calculated using the parabolic fit of eq. (4.5) for $\alpha^2 + \beta^2$. The alternative expressions (4.6) were used to check the consistency of the results in the range of temperature values where the power series method does not converge. In this case, the number of significant figures retained in $\widetilde{\omega}_I$ was chosen so that all the alternative ways of determining $\widetilde{\omega}_I$ give the same value.

In figure 6, we show our results for the square of the real and imaginary parts of the QN frequencies as functions of $\widetilde{T}^2$ for the first five modes $n = 0$, 1, ..., 4 with $q = 0$. We observe that, in the zero temperature limit, the real part of the QN frequencies coincide with the corresponding glueball mass spectrum, given by eq. (2.4). Then, increasing the temperature $\widetilde{\omega}_R^2$ decrease until they reach a minimum value $(\widetilde{\omega}_R^2)^{\min}$ at some critical tem-

JHEP11(2009)119

n	$\widetilde{T}^2$	$(\widetilde{\omega}_R^2)^{\min}$	$\widetilde{\omega}_I^2$	Q
0	0.122069	6.85489	0.108102	3.98156
1	0.0637774	9.92861	0.166347	3.86284
2	0.0444836	13.0406	0.241963	3.67066
3	0.0343047	16.1605	0.319899	3.55378
4	0.0279468	19.2844	0.398241	3.47936

Table 2. The minimum value of the real part of QN frequency for the first five modes, $n = 0, 1, \ldots, 4$, and the corresponding values of $\widetilde{\omega}_I^2$, $\widetilde{T}^2$, and the quality factor Q.

perature, different for each mode. The value of the critical temperature is lower for higher overtone numbers n. For higher temperatures, $\widetilde{\omega}_R$ increases approaching a linear dependence on the temperature. On the other hand, we observe in figure 6 that (the negative of) the imaginary part of the frequencies $\widetilde{\omega}_I$ increase monotonically with the temperature approaching constant slopes. In table 2, we show the values of the minimum of the curve $\widetilde{\omega}_R^2$ versus $\widetilde{T}^2$ for the first five quasinormal modes. We also show there the numerical values for $\widetilde{\omega}_I^2$ and the quality factor $Q = \omega_R/2\omega_I$ evaluated at the critical temperatures. Notice that the values of Q in the minimum of $\widetilde{\omega}_R$ are such that $Q \lesssim 4$ and so, for temperatures equal or higher than the critical value, there are no more quasiparticle peaks corresponding to glueballs in the spectral function $\mathcal{R}(\widetilde{\omega}, 0)$. Quasiparticle states show up for higher values of Q.

The decreasing of the real part of the quasinormal frequencies at very low temperatures, shown in figure 6, is related to the fact that the very low temperature potential given by (2.32) behaves as a harmonic oscillator with an infinite barrier r_*^{-2} and a temperature dependent negative correction $-T^4 r_*^6$. This negative correction is responsible for the observed decrease in $\widetilde{\omega}_R^2$ for $\widetilde{T}^2 \lesssim 0.1$.

The exact way the functions $\widetilde{\omega}_R^2(\widetilde{T}^2)$ and $\widetilde{\omega}_I^2(\widetilde{T}^2)$ deviate from the linear behavior, observed in high temperatures, varies with the level n. Within a certain accuracy, the frequency of each mode deviates significantly from a straight line only in the low temperature regime. For instance, this deviation for the fundamental mode occurs below $\widetilde{T}^2 = 0.25$. For higher overtones, as n increases, the deviations from the linear behavior occur at decreasing temperatures.

We now compare our results for the soft-wall model with the pure AdS black-hole case, which corresponds to the limit $\Phi = 0$. Some results for the fundamental mode ($n = 0$) obtained with the Horowitz-Hubeny power series method are shown in table 3 for $q = 0$ and selected values of temperature $\widetilde{T}$. We introduce for the real and imaginary parts of the QN frequencies the fractional differences

$$\Delta_{R,I} = \frac{|\omega_{R,I} - \omega_{R,I}^{\Phi=0}|}{\omega_{R,I}^{\Phi=0}} = \frac{|\mathfrak{w}_{R,I} - \mathfrak{w}_{R,I}^{\Phi=0}|}{\mathfrak{w}_{R,I}^{\Phi=0}}, \tag{4.8}$$

where $\mathfrak{w} = \omega/2\pi T$ is the normalized frequency commonly used in the literature [36, 47, 48] and the superscript $\Phi = 0$ indicates the results for the AdS black hole without dilaton.

JHEP11(2009)119

$\widetilde{T}^2$	$\widetilde{\omega}_R^2$	$\widetilde{\omega}_I^2$	Δ_R	Δ_I	Q
100	976.020	750.874	0.00150017	0.0023548	0.570054
25	246.247	185.138	0.0060918	0.00923686	0.576645
4	42.1859	27.1783	0.0410586	0.0509827	0.622934
1	13.6137	5.45053	0.182798	0.150013	0.790204
0.25	7.40192	0.672991	0.744311	0.402652	1.65820
0.04	7.72086	1.31516×10^{-6}	3.45374	0.997912	1211.47

Table 3. The frequencies of the fundamental QNM for some selected values of temperature $\widetilde{T}$, calculated with $q = 0$. We also show the fractional differences in relation to the frequency values in the absence of dilaton, Δ_R and Δ_I, and the quality factor of the oscillations, Q.

Since the frequencies $\mathfrak{w}_R^{\Phi=0}$ and $\mathfrak{w}_I^{\Phi=0}$ are constants independent of the temperature, for a fixed level n the fractional differences $\Delta_{R,I}$ varies with $\widetilde{T}$ due to the changes in the values of $\mathfrak{w}_{R,I} = \widetilde{\omega}_{R,I}/2\widetilde{T}$.

As expected, one can see a significant difference in the numerical results for the soft-wall and pure AdS cases for low temperatures. For higher values of $\widetilde{T}$, the effect of the background dilaton field is small, and the QNMs are essentially the same as those of the pure black hole solution [46, 47]. This is related to the fact that the effective potential $V(r_*)$ is a monotonic function without wells both in the intermediate- and high-temperature regimes.

4.2.2 Dispersion relations

In this section we investigate the momentum dependence of the scalar-field black hole quasinormal modes in the soft-wall model. In table 4, we list some of our numerical results for the real and (negative of) imaginary parts of the QN frequencies, $\omega_R(q)$ and $\omega_I(q)$, for selected values of $\widetilde{T}$ and two different momenta, $\widetilde{q} = 1, 10$. We also compare $\omega_R(q)$ with the standard relativistic dispersion relation $\omega = \sqrt{(\omega_R^0)^2 + q^2}$, where $\omega_R^0 \equiv \omega_R(q)|_{q=0}$ can be regarded as the glueball mass at finite temperature. We introduce the fractional difference

$$\Delta_q = \frac{|\omega_R(q) - \sqrt{(\omega_R^0)^2 + q^2}|}{\sqrt{(\omega_R^0)^2 + q^2}}, \tag{4.9}$$

which is a measure of the fractional difference between the numerical values obtained for ω_R and the relativistic energy-momentum relation for a massive particle.

In the ranges of momentum and temperature considered here we have obtained very small values for Δ_q. The maximum value found for this quantity corresponds approximately to 1.3 %, and appears for $\widetilde{q} = 10$ and $\widetilde{T}^2 = 0.2$. The overall behavior of the dispersion relation $\omega_R(q)$ is such that Δ_q increases with the momentum and presents an oscillatory dependence in $\widetilde{T}$ for low temperatures, while increases monotonically for higher $\widetilde{T}$.

We present in figure 7 the variation of the real and (negative of) imaginary parts of the QN frequency with the momentum for selected values of the temperature. In the left panel of this figure, we illustrate the behaviour of the real part of the frequency in the

JHEP11(2009)119

	$\widetilde{q}=1$			$\widetilde{q}=10$		
$\widetilde{T}^2$	$\widetilde{\omega}_R$	$\widetilde{\omega}_I$	Δ_q	$\widetilde{\omega}_R$	$\widetilde{\omega}_I$	Δ_q
0.2	2.85042	0.644367	0.0010234	10.4808	0.562306	0.0127022
0.15	2.80845	0.452717	0.000665236	10.4244	0.449494	0.00824847
0.1	2.80271	0.231549	0.0024438	10.3660	0.317525	0.00262035
0.05	2.91009	0.0157488	0.00267834	10.3162	0.143700	0.00508183

Table 4. Some data for the fundamental QN frequency of the glueball fluctuations for $\widetilde{q}=1$, 10 and selected values of temperature.

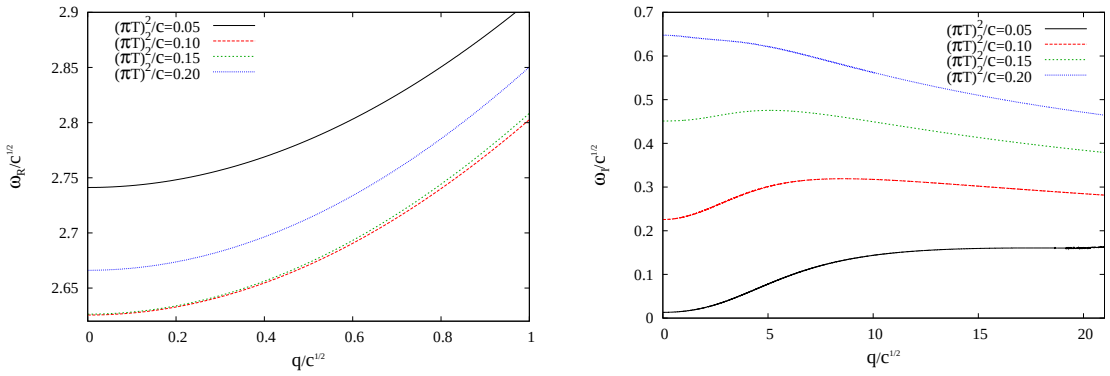

Figure 7. The dispersion relations of the fundamental quasinormal mode $n=0$ for some selected values of temperature.

$\widetilde{T}^2$	$\widetilde{q}$	$\widetilde{\omega}_R$	$\widetilde{\omega}_I^{\max}$	τ
0.20	0	2.66613	0.647625	1.54410
0.15	5.1149	5.77971	0.475506	2.10302
0.10	8.5667	8.9751	0.319018	3.13462

Table 5. The maximum absolute value of the imaginary part of the fundamental QN frequency as a function of $\widetilde{q}$, the corresponding values of $\widetilde{\omega}_R$, $\widetilde{T}^2$, and the characteristic damping time $\tau=1/\omega_I$ in units of $c^{-1/2}$. The numerical methods used here present bad convergence for $\widetilde{T}^2 \lesssim 0.05$.

range $0 \leq \widetilde{q} \leq 1$. From this picture, one can see that $\widetilde{\omega}_R(\widetilde{q})$ increases with the momentum. In our study we found this behaviour for all temperatures investigated.

In the right panel of figure 7, we show the dependence of (the negative of) the imaginary part of the frequencies with the momentum. The power series method converged well for momenta in the range $0 < \widetilde{q} \lesssim 40$ and $\widetilde{T}^2 = 0.2$, but only for $0 < \widetilde{q} \lesssim 20$ when $\widetilde{T}^2 = 0.05$. We found that the absolute value of the imaginary part of the frequency presents a maximum value, which means a minimum for $\tau = 1/\omega_I$, for some finite momentum. For temperatures above a critical value $\widetilde{T}^2 \approx 0.16$, the maximum value of $\widetilde{\omega}_I$ is achieved at $\widetilde{q}=0$. For temperatures below this critical value, $\widetilde{\omega}_I$ increases with the momentum for very

JHEP11(2009)119

low $\widetilde{q}$'s, reaches a maximum value $\widetilde{\omega}_I^{max}$ and then decreases monotonically. Our numerical results suggest that $\widetilde{\omega}_I$ vanishes for infinitely large $\widetilde{q}$, a behavior similar to that of the pure AdS black hole case investigated in refs. [60, 61].

In table 5, for some selected temperatures $\widetilde{T}$, we present the maximum values of $\widetilde{\omega}_I$ and the corresponding values of $\widetilde{q}$, $\widetilde{\omega}_R$, and the thermalization timescale $\tau = 1/\widetilde{\omega}_I^{max}$. Below the temperature $\widetilde{T}^2 = 0.05$ the convergence of our numerical methods gets weak, and we could not determine the value of $\widetilde{\omega}_I^{max}$ for $\widetilde{T}^2 \leq 0.05$. In the AdS black hole space without the dilaton, the (negative of the) imaginary part of the frequency is a decreasing function of the momentum q [46, 47], which is in accordance with the behavior of $\widetilde{\omega}_I$ for $\widetilde{T}^2 > 0.16$.

5 Final comments and conclusion

In this article we investigated the spectrum of scalar glueballs at finite temperature in the soft-wall model. Such a study was performed considering a scalar field in an AdS black hole spacetime in the presence of a dilaton field as the gravity dual of finite temperature scalar glueballs. This background corresponds to the deconfined plasma phase which is thermodynamically favoured at high temperatures. We considered here the AdS black hole space for all temperatures. For intermediate temperatures it represents a supercooled metastable (positive specific heat) plasma and for low temperatures an unstable (negative specific heat) plasma.

We obtained the thermal and momentum dependences of the frequencies of the black-hole quasinormal modes. For $q = 0$, the real part of the QN frequencies furnishes the glueball masses for low temperatures. In the zero temperature limit our results give the glueball spectrum found in ref. [19] for the soft-wall model. Surprisingly, for very low temperatures and low fixed momentum, these masses decrease with increasing temperature. After reaching a minimum value, the real part of the QN frequencies grows monotonically with the temperature, as in the case without the dilaton field.

At zero temperature there is an infinite number of stable glueball states corresponding to delta function peaks in the spectral function. As the temperature increases, however, the peaks spread, and for a fixed low temperature and fixed low momentum, there is only a finite number of sharp peaks, since the width of the peaks increase with the frequency. The sharp peaks correspond to QNMs whose complex frequencies have small imaginary parts. These modes can be interpreted as glueball quasiparticle states with decay rates inversely proportional to the imaginary part of the frequencies. This imaginary part is also proportional to the width of the peak of the spectral function.

We studied the dispersion relations for the glueballs in the soft wall at finite temperature. This way we found the effect of the quasiparticle motion on its lifetime inside the plasma. The connection of the complex QN frequencies with the mass and the decaying time of quasiparticles in the dual plasma gives an important tool to explore both sides of the duality using known elements from the gauge theory and the physics of black holes.

The process of spreading of a peak as the temperature increases is interpreted as the melting of the quasiparticles in the thermal bath. We found that the scalar glueball states melt at temperatures much lower than the confinement/deconfinement temperature. In

JHEP11(2009)119

the soft-wall model the phase transition occurs at $T = T_c$ with $(\pi T_c)^2/c \approx 2.39$, while we found that, at $(\pi T)^2/c \approx 0.1$ all the quasiparticles have melted.

Our results indicate that the glueball formation in the black hole phase occurs at very low temperatures compared to the deconfinement temperature. So, from the point of view of the soft-wall model, it would be difficult to observe experimentally the contribution of the black hole phase to glueball formation unless the plasma cools down in a very small time scale, compared to that of the thermal phase transition. Recall that in the soft-wall model there are two different thermal phases, corresponding to different backgrounds. As shown in ref. [22] there is a first order phase transition between them, implying that these two phases can coexist. For $T < T_c$, the thermal AdS space without a black hole is dominant. In this confining background the glueballs are formed at temperatures just below T_c having constant masses and zero widths.

As already mentioned, the soft-wall model is not a solution of the 5D Einstein equations since it does not take into account the dilaton backreaction. There are some recent AdS/QCD models at zero temperature that overcome this problem [62–64]. At finite temperature, the thermodynamics of AdS/QCD models with dilaton backreaction was considered in [65, 66]. It would be interesting to extend the analysis of the present work to these kind of models. This way one could distinguish the aspects that represent general characteristics of quasiparticle excitations in the plasma from those specific to the holographic soft-wall model considered here.

After completing this work we noticed the very recent article [67] where glueballs and mesons in the soft-wall model at finite temperature are studied, with some overlap with this work.

Acknowledgments

We thank Vitor Cardoso and Jaqueline Morgan for the help with the numerical methods employed in this work. We also thank Marcus A. C. Torres for stimulating conversations. The authors are partially supported by CNPq, Capes and Faperj, Brazilian agencies.

References

[1] J.M. Maldacena, *The large-N limit of superconformal field theories and supergravity*, *Adv. Theor. Math. Phys.* **2** (1998) 231 [*Int. J. Theor. Phys.* **38** (1999) 1113] [hep-th/9711200] [SPIRES].

[2] E. Witten, *Anti-de Sitter space and holography*, *Adv. Theor. Math. Phys.* **2** (1998) 253 [hep-th/9802150] [SPIRES].

[3] S.S. Gubser, I.R. Klebanov and A.M. Polyakov, *Gauge theory correlators from non-critical string theory*, *Phys. Lett.* **B 428** (1998) 105 [hep-th/9802109] [SPIRES].

[4] E. Witten, *Anti-de Sitter space, thermal phase transition and confinement in gauge theories*, *Adv. Theor. Math. Phys.* **2** (1998) 505 [hep-th/9803131] [SPIRES].

[5] D.T. Son and A.O. Starinets, *Minkowski-space correlators in AdS/CFT correspondence: recipe and applications*, *JHEP* **09** (2002) 042 [hep-th/0205051] [SPIRES].

JHEP11(2009)119

[6] C.P. Herzog and D.T. Son, *Schwinger-Keldysh propagators from AdS/CFT correspondence*, *JHEP* **03** (2003) 046 [hep-th/0212072] [SPIRES].

[7] K. Skenderis and B.C. van Rees, *Real-time gauge/gravity duality*, *Phys. Rev. Lett.* **101** (2008) 081601 [arXiv:0805.0150] [SPIRES].

[8] K. Skenderis and B.C. van Rees, *Real-time gauge/gravity duality: prescription, renormalization and examples*, *JHEP* **05** (2009) 085 [arXiv:0812.2909] [SPIRES].

[9] E. Berti, V. Cardoso and A.O. Starinets, *Quasinormal modes of black holes and black branes*, *Class. Quant. Grav.* **26** (2009) 163001 [arXiv:0905.2975] [SPIRES].

[10] H. Boschi-Filho and N.R.F. Braga, *QCD/String holographic mapping and glueball mass spectrum*, *Eur. Phys. J.* **C 32** (2004) 529 [hep-th/0209080] [SPIRES].

[11] H. Boschi-Filho and N.R.F. Braga, *Gauge/string duality and scalar glueball mass ratios*, *JHEP* **05** (2003) 009 [hep-th/0212207] [SPIRES].

[12] G.F. de Teramond and S.J. Brodsky, *The hadronic spectrum of a holographic dual of QCD*, *Phys. Rev. Lett.* **94** (2005) 201601 [hep-th/0501022] [SPIRES].

[13] J. Erlich, E. Katz, D.T. Son and M.A. Stephanov, *QCD and a holographic model of hadrons*, *Phys. Rev. Lett.* **95** (2005) 261602 [hep-ph/0501128] [SPIRES].

[14] L. Da Rold and A. Pomarol, *Chiral symmetry breaking from five dimensional spaces*, *Nucl. Phys.* **B 721** (2005) 79 [hep-ph/0501218] [SPIRES].

[15] H. Boschi-Filho, N.R.F. Braga and H.L. Carrion, *Glueball Regge trajectories from gauge/string duality and the Pomeron*, *Phys. Rev.* **D 73** (2006) 047901 [hep-th/0507063] [SPIRES].

[16] H. Boschi-Filho, N.R.F. Braga and C.N. Ferreira, *Heavy quark potential at finite temperature from gauge/string duality*, *Phys. Rev.* **D 74** (2006) 086001 [hep-th/0607038] [SPIRES].

[17] H. Boschi-Filho, N.R.F. Braga and C.N. Ferreira, *Static strings in Randall-Sundrum scenarios and the quark anti-quark potential*, *Phys. Rev.* **D 73** (2006) 106006 [*Erratum ibid.* **D 74** (2006) 089903] [hep-th/0512295] [SPIRES].

[18] A. Karch, E. Katz, D.T. Son and M.A. Stephanov, *Linear confinement and AdS/QCD*, *Phys. Rev.* **D 74** (2006) 015005 [hep-ph/0602229] [SPIRES].

[19] P. Colangelo, F. De Fazio, F. Jugeau and S. Nicotri, *On the light glueball spectrum in a holographic description of QCD*, *Phys. Lett.* **B 652** (2007) 73 [hep-ph/0703316] [SPIRES].

[20] P. Colangelo, F. De Fazio, F. Giannuzzi, F. Jugeau and S. Nicotri, *Light scalar mesons in the soft-wall model of AdS/QCD*, *Phys. Rev.* **D 78** (2008) 055009 [arXiv:0807.1054] [SPIRES].

[21] O. Andreev and V.I. Zakharov, *The spatial string tension, thermal phase transition and AdS/QCD*, *Phys. Lett.* **B 645** (2007) 437 [hep-ph/0607026] [SPIRES].

[22] C.P. Herzog, *A holographic prediction of the deconfinement temperature*, *Phys. Rev. Lett.* **98** (2007) 091601 [hep-th/0608151] [SPIRES].

[23] K. Kajantie, T. Tahkokallio and J.-T. Yee, *Thermodynamics of AdS/QCD*, *JHEP* **01** (2007) 019 [hep-ph/0609254] [SPIRES].

[24] C.A. Ballon Bayona, H. Boschi-Filho, N.R.F. Braga and L.A. Pando Zayas, *On a holographic model for confinement/deconfinement*, *Phys. Rev.* **D 77** (2008) 046002 [arXiv:0705.1529] [SPIRES].

JHEP11(2009)119

[25] S.W. Hawking and D.N. Page, *Thermodynamics of black holes in Anti-de Sitter space*, *Commun. Math. Phys.* **87** (1983) 577 [SPIRES].

[26] R.C. Myers, A.O. Starinets and R.M. Thomson, *Holographic spectral functions and diffusion constants for fundamental matter*, *JHEP* **11** (2007) 091 [arXiv:0706.0162] [SPIRES].

[27] G.T. Horowitz and V.E. Hubeny, *Quasinormal modes of AdS black holes and the approach to thermal equilibrium*, *Phys. Rev.* **D 62** (2000) 024027 [hep-th/9909056] [SPIRES].

[28] E. Berti, V. Cardoso and P. Pani, *Breit-Wigner resonances and the quasinormal modes of Anti-de Sitter black holes*, *Phys. Rev.* **D 79** (2009) 101501 [arXiv:0903.5311] [SPIRES].

[29] H. Forkel, *Holographic glueball structure*, *Phys. Rev.* **D 78** (2008) 025001 [arXiv:0711.1179] [SPIRES].

[30] V. Mathieu, N. Kochelev and V. Vento, *The physics of glueballs*, *Int. J. Mod. Phys.* **E 18** (2009) 1 [arXiv:0810.4453] [SPIRES].

[31] G. Gibbons and S.A. Hartnoll, *A gravitational instability in higher dimensions*, *Phys. Rev.* **D 66** (2002) 064024 [hep-th/0206202] [SPIRES].

[32] H. Kodama and A. Ishibashi, *A master equation for gravitational perturbations of maximally symmetric black holes in higher dimensions*, *Prog. Theor. Phys.* **110** (2003) 701 [hep-th/0305147] [SPIRES].

[33] J. Morgan, V. Cardoso, A.S. Miranda, C. Molina and V.T. Zanchin, *Gravitational quasinormal modes of AdS black branes in d spacetime dimensions*, *JHEP* **09** (2009) 117 [arXiv:0907.5011] [SPIRES].

[34] M. Bianchi, D.Z. Freedman and K. Skenderis, *Holographic renormalization*, *Nucl. Phys.* **B 631** (2002) 159 [hep-th/0112119] [SPIRES].

[35] M. Fujita, K. Fukushima, T. Misumi and M. Murata, *Finite-temperature spectral function of the vector mesons in an AdS/QCD model*, *Phys. Rev.* **D 80** (2009) 035001 [arXiv:0903.2316] [SPIRES].

[36] P. Kovtun and A. Starinets, *Thermal spectral functions of strongly coupled $N = 4$ supersymmetric Yang-Mills theory*, *Phys. Rev. Lett.* **96** (2006) 131601 [hep-th/0602059] [SPIRES].

[37] D. Teaney, *Finite temperature spectral densities of momentum and R-charge correlators in $N = 4$ Yang-Mills theory*, *Phys. Rev.* **D 74** (2006) 045025 [hep-ph/0602044] [SPIRES].

[38] R.C. Myers and A. Sinha, *The fast life of holographic mesons*, *JHEP* **06** (2008) 052 [arXiv:0804.2168] [SPIRES].

[39] R.C. Myers and M.C. Wapler, *Transport properties of holographic defects*, *JHEP* **12** (2008) 115 [arXiv:0811.0480] [SPIRES].

[40] P. Colangelo, F. De Fazio, F. Jugeau and S. Nicotri, *Investigating AdS/QCD duality through scalar glueball correlators*, *Int. J. Mod. Phys.* **A 24** (2009) 4177 [arXiv:0711.4747] [SPIRES].

[41] K.D. Kokkotas and B.G. Schmidt, *Quasi-normal modes of stars and black holes*, *Living Rev. Rel.* **2** (1999) 2 [gr-qc/9909058] [SPIRES].

[42] H.P. Nollert, *Topical review: quasinormal modes: the characteristic 'sound' of black holes and neutron stars*, *Class. Quant. Grav.* **16** (1999) R159 [SPIRES].

JHEP11(2009)119

[43] B. Wang, C. Molina and E. Abdalla, *Evolving of a massless scalar field in Reissner-Nordström Anti-de Sitter spacetimes*, *Phys. Rev.* **D 63** (2001) 084001 [hep-th/0005143] [SPIRES].

[44] V. Cardoso and J.P.S. Lemos, *Scalar, electromagnetic and Weyl perturbations of BTZ black holes: quasi normal modes*, *Phys. Rev.* **D 63** (2001) 124015 [gr-qc/0101052] [SPIRES].

[45] V. Cardoso and J.P.S. Lemos, *Quasi-normal modes of Schwarzschild Anti-de Sitter black holes: electromagnetic and gravitational perturbations*, *Phys. Rev.* **D 64** (2001) 084017 [gr-qc/0105103] [SPIRES].

[46] A.O. Starinets, *Quasinormal modes of near extremal black branes*, *Phys. Rev.* **D 66** (2002) 124013 [hep-th/0207133] [SPIRES].

[47] A. Núñez and A.O. Starinets, *AdS/CFT correspondence, quasinormal modes and thermal correlators in $N = 4$ SYM*, *Phys. Rev.* **D 67** (2003) 124013 [hep-th/0302026] [SPIRES].

[48] P.K. Kovtun and A.O. Starinets, *Quasinormal modes and holography*, *Phys. Rev.* **D 72** (2005) 086009 [hep-th/0506184] [SPIRES].

[49] K. Maeda, M. Natsuume and T. Okamura, *Quasinormal modes for nonextreme Dp-branes and thermalizations of super-Yang-Mills theories*, *Phys. Rev.* **D 72** (2005) 086012 [hep-th/0509079] [SPIRES].

[50] G. Siopsis, *On quasi-normal modes and the AdS_5/CFT_4 correspondence*, *Nucl. Phys.* **B 715** (2005) 483 [hep-th/0407157] [SPIRES].

[51] A.S. Miranda and V.T. Zanchin, *Quasinormal modes of plane-symmetric anti-de Sitter black holes: a complete analysis of the gravitational perturbations*, *Phys. Rev.* **D 73** (2006) 064034 [gr-qc/0510066] [SPIRES].

[52] Y. Zhang and J.-L. Jing, *Quasinormal frequencies of the Rarita-Schwinger field in Reissner-Nordström-Anti-de Sitter space-time*, *Int. J. Mod. Phys.* **D 15** (2006) 905 [SPIRES].

[53] C. Hoyos-Badajoz, K. Landsteiner and S. Montero, *Holographic meson melting*, *JHEP* **04** (2007) 031 [hep-th/0612169] [SPIRES].

[54] A.S. Miranda and V.T. Zanchin, *Gravitational perturbations and quasinormal modes of black holes with non-spherical topology*, *Int. J. Mod. Phys.* **D 16** (2007) 421 [SPIRES].

[55] I. Amado and C. Hoyos-Badajoz, *AdS black holes as reflecting cavities*, *JHEP* **09** (2008) 118 [arXiv:0807.2337] [SPIRES].

[56] G.B. Arfken and H.J. Weber, *Mathematical methods for physicists*, 4th edition, Academic Press, San Diego U.S.A. (1995).

[57] K.S. Thorne, *Nonradial pulsation of general-relativistic stellar models. III. Analytic and numerical results for neutron stars*, *Astrophys. J.* **158** (1969) 1.

[58] S. Chandrasekhar and V. Ferrari, *On the non-radial oscillations of a star. III: a reconsideration of the axial modes*, *Proc. Roy. Soc. Lond.* **A 434** (1991) 449.

[59] S. Chandrasekhar and V. Ferrari, *On the non-radial oscillations of a star. IV: an application of the theory of Regge poles*, *Proc. Roy. Soc. Lond.* **A 437** (1992) 133.

[60] G. Festuccia and H. Liu, *A Bohr-Sommerfeld quantization formula for quasinormal frequencies of AdS black holes*, arXiv:0811.1033 [SPIRES].

JHEP11(2009)119

[61] J. Morgan, V. Cardoso, A.S. Miranda, C. Molina and V.T. Zanchin, *Quasinormal modes of black holes in Anti-de Sitter space: a numerical study of the eikonal limit*, *Phys. Rev.* **D 80** (2009) 024024 [arXiv:0906.0064] [SPIRES].

[62] U. Gürsoy and E. Kiritsis, *Exploring improved holographic theories for QCD: part I*, *JHEP* **02** (2008) 032 [arXiv:0707.1324] [SPIRES].

[63] U. Gürsoy, E. Kiritsis and F. Nitti, *Exploring improved holographic theories for QCD: part II*, *JHEP* **02** (2008) 019 [arXiv:0707.1349] [SPIRES].

[64] W. de Paula, T. Frederico, H. Forkel and M. Beyer, *Dynamical AdS/QCD with area-law confinement and linear Regge trajectories*, *Phys. Rev.* **D 79** (2009) 075019 [arXiv:0806.3830] [SPIRES].

[65] U. Gürsoy, E. Kiritsis, L. Mazzanti and F. Nitti, *Holography and thermodynamics of* $5D$ *dilaton-gravity*, *JHEP* **05** (2009) 033 [arXiv:0812.0792] [SPIRES].

[66] U. Gürsoy, E. Kiritsis, L. Mazzanti and F. Nitti, *Deconfinement and gluon plasma dynamics in improved holographic QCD*, *Phys. Rev. Lett.* **101** (2008) 181601 [arXiv:0804.0899] [SPIRES].

[67] P. Colangelo, F. Giannuzzi and S. Nicotri, *Holographic approach to finite temperature QCD: the case of scalar glueballs and scalar mesons*, arXiv:0909.1534 [SPIRES].

JHEP11(2009)119